

# Ergodic capacity analysis of reconfigurable intelligent surface assisted wireless systems

Alexandros–Apostolos A. Boulogeorgos, and Angeliki Alexiou  
 Department of Digital Systems, University of Piraeus, Piraeus, Greece  
 E-mails: al.boulogeorgos@ieee.org, alexiou@unipi.gr

**Abstract**—This paper presents the analytic framework for evaluating the ergodic capacity (EC) of the reconfigurable intelligent surface (RIS) assisted systems. Moreover, high-signal-to-noise-ratio and high-number of reflection units (RUs) approximations for the EC are provided. Finally, the special case in which the RIS is equipped with a single RU is investigated. Our analysis is verified through respective Monte Carlo simulations, which highlight the accuracy of the proposed framework.

**Index Terms**—Ergodic capacity, High-signal-to-noise-ratio approximation, Performance analysis, Reconfigurable intelligent surfaces.

## I. INTRODUCTION

While the wireless world moves towards the sixth generation (6G) era, the data-rate and network traffic demands have been exponential increased [1]–[4]. Technological advances, such as massive multiple-input multiple-output, full-duplexing, and high-frequency communications, have been advocated, due to the power consumption increase that they cause [5]–[8], as well as their performance limitations when operating in unfavorable wireless propagation environment [9]–[13].

To surpass the aforementioned issues, the use of reconfigurable intelligent surfaces (RISs) in order to exploit the implicit randomness of the propagation environment have attracted the attention of both academia and industry [14]. Most RISs consist of two dimensional reflection units (RUs) arrays, which are controlled by at least one micro-controller, and can alter the incoming electromagnetic (EM) field [15]. In particular, each RU can independently change the phase of the incident EM wave; hence, they are able to collaboratively create a favorable wireless channel [16].

Scanning the open literature, the performance analysis of RIS-assisted systems is a topic of much hype (see e.g., [17]–[21] and references therein). Specifically, in [17] and [18], [22], the authors provided a symbol error rate (SER) bound for RIS-assisted systems. Note that these upper-bounds are quite tight for RIS utilizations with high-number of RUs, but, in the low-RUs regime, they are not so accurate. Similarly, in [19], an error analysis was provided for RIS-assisted non-orthogonal multiple

access systems. Again, the authors employed the central limit theorem for approximating the distribution of the equivalent wireless channel. As a consequence, the results are accurate only for scenarios, in which the RIS consists of a large-number of RUs. In [20], the authors presented an asymptotic analysis of the uplink sum-rate of a RIS-assisted system, assuming that the established channels follow Rician distribution. Finally, in [22], the performance of such systems in terms of energy efficiency was quantified.

To the best of the authors knowledge, no analytical assessment of the EC in RIS-assisted systems has been reported. Motivated by this, this work presents the analytical framework that quantifies the EC of RIS-assisted systems. In this sense, we initially present novel a closed-form expression for the probability density function (PDF) of the end-to-end (e2e) fading channel coefficient of the RIS-assisted system. Moreover, the PDF of the e2e fading channel for the special case, in which the RIS is equipped with a single RU, is also presented. Building upon them, we extract closed-form expressions for the EC of the RIS-assisted system for both cases, in which the RIS is equipped with multiple and a single RU. Finally, tight novel high-SNR and high-RU number approximations for the EC are derived.

**Notations:** The operators  $\mathbb{E}[\cdot]$ ,  $\mathbb{V}[\cdot]$  and  $|\cdot|$  respectively denote the statistical expectation, variance, and the absolute value, whereas  $\exp(x)$  and  $\log_2(x)$  respectively stand for the exponential and the binary logarithmic functions. Additionally,  $\ln(x)$  refers to the natural logarithm of  $x$ , while  $\sqrt{x}$  and  $\lim_{x \rightarrow a} (f(x))$  respectively return the square root of  $x$  and the limit of the function  $f(x)$  as  $x$  tends to  $a$ . Furthermore,  $(x)_n$  denotes the Pochhammer operator. Also,  $\csc(x)$  and  $\sec(x)$  respectively return the cosecant and the secant of  $x$ . The upper and lower incomplete Gamma functions [23, eq. (8.350/2), (8.350/3)] are respectively denoted by  $\Gamma(\cdot, \cdot)$  and  $\gamma(\cdot, \cdot)$ , while the Gamma function is represented by  $\Gamma(\cdot)$  [23, eq. (8.310)], whereas  $K_v(\cdot)$  and  $I_v(\cdot)$  are respectively the modified Bessel function of the second [24, eq. (9.6.2)] and first kind of order  $v$  [24, eq. (9.6.3)]. Moreover,  $F_0(\cdot)$ ,  $E(\cdot)$ , and  $K(\cdot)$  respectively represent the polygamma function of the zero order [24, eq. (6.4.1)], the elliptic integral function [24, eq. (17.1.1)],

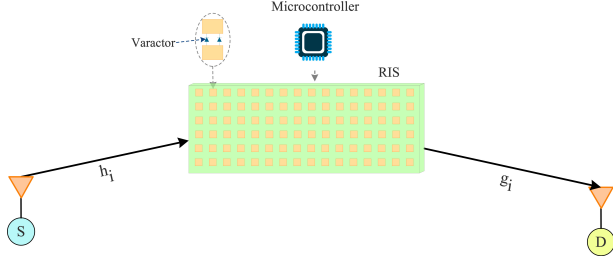


Fig. 1: System model of the RIS-assisted wireless system.

and the complete elliptic integral function of the first kind [24, eq. (17.3.1)]. Furthermore,  ${}_2F_1(\cdot, \cdot; \cdot; \cdot)$  stands for the Gauss hypergeometric function [24, eq. (4.1.1)], while  ${}_pF_q(a_1, \dots, a_p; b_1, \dots, b_q; x)$  is the generalized hypergeometric function [23, eq. (9.14/1)]. Meanwhile,  $U(a, b, x)$  and  $G_{p,q}^{m,n}\left(x \left| \begin{matrix} a_1, a_2, \dots, a_p \\ b_1, b_2, \dots, b_q \end{matrix} \right. \right)$  respectively represent the confluent hypergeometric function of second kind [23, ch. 9.2], and the Meijer's G-function [23, eq. (9.301)].

## II. SYSTEM MODEL

As shown in Fig. 1, we consider a RIS-assisted wireless system, in which a single-antenna source (S) node communicates with a single-antenna destination (D) node through a RIS, that consists of  $N$  RUs. The baseband equivalent channels between S and the  $i$ -th RU of the RIS,  $h_i$ , as well as the one between the  $i$ -th RU and D,  $g_i$ , are assumed to be independent and Rayleigh distributed random variables (RVs) with scale parameters 1. This assumption originates from the fact that even if the line-of-sight links between S-RIS and RIS-D are blocked, there still exist extensive scatters. Moreover, as usual practice, in this work, we also neglect the deterministic path-gain in the fading coefficients  $h_i$  and  $g_i$ .

Hence, the baseband equivalent received signal at D is given by

$$y = \sum_{i=1}^N h_i g_i r_i x + n, \quad (1)$$

where  $n$  denotes the additive white Gaussian noise and can be modeled as a zero-mean complex Gaussian RV with variance equal  $N_0$ . Likewise,  $r_i$  represents the  $i$ -th RU response and can be expressed as

$$r_i = |r_i| \exp(j\theta_i), \quad (2)$$

with  $\theta_i$  being the PS applied by the  $i$ -th reflecting RU of the RIS. In this work, we assume that the phases of the channels  $h_i$  and  $g_i$  are perfectly known to the RIS, and that thus the RIS selects the optimal phase shifting, which is  $\theta_i = -(\phi_{h_i} + \phi_{g_i})$ , where  $\phi_{h_i}$  and  $\phi_{g_i}$  are respectively the phases of  $h_i$  and  $g_i$ . In addition, without

loss of generality, it is assumed that the reflected gain of the  $i$ -th RU,  $|r_i|$ , is equal to 1. Hence, (2) can be simplified as

$$r_i = \exp(-j(\phi_{h_i} + \phi_{g_i})). \quad (3)$$

By employing (3), (1) can be expressed as

$$y = Ax + n, \quad (4)$$

where

$$A = \sum_{i=1}^N |h_i| |g_i|. \quad (5)$$

## III. PERFORMANCE ANALYSIS

The following theorem returns closed-form approximation for the PDF and CDF of  $A$ .

**Lemma 1.** *The PDF of  $A$  can be evaluated as*

$$f_A(x) = \frac{x^a}{b^{a+1} \Gamma(a+1)} \exp\left(-\frac{x}{b}\right), \quad (6)$$

where

$$a = \frac{k_1^2}{k_2} - 1, \text{ and } b = \frac{k_2}{k_1}, \quad (7)$$

with

$$k_1 = \frac{N\pi}{2}, \text{ and } k_2 = 4N \left(1 - \frac{\pi^2}{16}\right). \quad (8)$$

*Proof:* Please refer to Appendix A. ■

**Special case:** For the case in which the RIS consists of a single RU, i.e.  $N = 1$ ,  $A$  is the product of two independent and identical Rayleigh distributed random variables (RVs); thus, it follows a double Rayleigh distribution and its PDF can be obtained as [25, eq. (3)]

$$f_A^s = x K_0(x). \quad (9)$$

The following theorem return a novel closed-form expression for the EC.

**Theorem 1.** *The EC of the RIS-assisted system can be analytically computed as in (10), given at the top of the next page. In (10),  $\rho_t = \frac{P_t}{N_0}$ , where  $P_t$  is the S transmission power.*

*Proof:* Please refer to Appendix B. ■

The following corollaries present high-SNR and high- $N$  approximations for the EC.

**Corollary 1.** *In the high SNR regime, the EC can be approximated as in (11), given at the top of the next page.*

*Proof:* For  $\rho_t \rightarrow \infty$ ,  $y = \frac{1}{4b^2\rho_t} \rightarrow 0$ . Moreover,

$$\lim_{y \rightarrow 0} {}_1F_2\left(1 + \frac{a}{2}; \frac{3}{2}, 2 + \frac{a}{2}, -y\right) = 1, \quad (12)$$

$$\lim_{y \rightarrow 0} {}_1F_2\left(\frac{a+1}{2}; \frac{1}{2}, \frac{a+3}{2}, -y\right) = 1 \quad (13)$$

$$C = \frac{a^2 - a}{(a-1)_2} \log_2(b^2 \rho_s) + \frac{2(a^2 - a)}{\ln(2)(a-1)_2} F_0(3+a) + \frac{\pi \csc\left(\frac{a\pi}{2}\right) {}_1F_2\left(1 + \frac{a}{2}; \frac{3}{2}, 2 + \frac{a}{2}, -\frac{1}{4b^2 \rho_s}\right)}{\ln(2)(2+a)b^{a+2}\Gamma(a+1)\rho_s^{\frac{a}{2}+1}} \\ + \frac{\pi \sec\left(\frac{a\pi}{2}\right) {}_1F_2\left(\frac{a+1}{2}; \frac{1}{2}, \frac{a+3}{2}, -\frac{1}{4b^2 \rho_s}\right)}{(a+1)b^{a+1} \ln(2) \Gamma(a+1) \rho_s^{\frac{a+1}{2}}} + \frac{{}_2F_3\left(1, 1; 2, 1 - \frac{a}{2}, \frac{3-a}{2}, -\frac{1}{4b^2 \rho_s}\right)}{\ln(2)(a-1)_2 b^2 \rho_s} \quad (10)$$

$$C_\rho \approx \frac{1}{\ln(2)(a-1)_2 b^2 \rho_t} + \frac{(a^2 - a) \log_2(b^2 \rho_t) + \frac{2(a^2 - a)}{\ln(2)(a-1)_2} F_0(3+a)}{(a-1)_2} \\ + \frac{\pi \csc\left(\frac{a\pi}{2}\right)}{\ln(2)(2+a)b^{a+2}\Gamma(a+1)\rho_t^{\frac{a}{2}+1}} + \frac{\pi \sec\left(\frac{a\pi}{2}\right)}{(a+1)b^{a+1} \ln(2) \Gamma(a+1) \rho_t^{\frac{a+1}{2}}} \quad (11)$$

and

$$\lim_{y \rightarrow 0} {}_2F_3\left(1, 1; 2, 1 - \frac{a}{2}, \frac{3-a}{2}, -y\right) = 1. \quad (14)$$

Thus, in the high SNR regime (10) can be approximated as in (11). This concludes the proof. ■

**Corollary 2.** *In the high SNR and  $N$  regime, the EC can be approximated as*

$$C_{\rho, N} \approx \frac{1}{\ln(2)(a-1)_2 b^2 \rho_t} + \frac{a^2 - a}{(a-1)_2} \log_2(b^2 \rho_t) \\ + \frac{2(a^2 - a)}{\ln(2)(a-1)_2} F_0(3+a). \quad (15)$$

*Proof:* In the high SNR regime, as  $N \rightarrow \infty$ ,  $a \rightarrow \infty$ ; hence, since  $\Gamma(a+1)$  is an increasing function, as  $N \rightarrow \infty$ ,  $\Gamma(a+1) \rightarrow \infty$ , or equivalently  $\frac{1}{\Gamma(a+1)} \rightarrow 0$ . This indicates  $\lim_{N \rightarrow \infty} \mathcal{B}_1 = \lim_{N \rightarrow \infty} \mathcal{B}_2 = 0$ , where

$$\mathcal{B}_1 = \frac{\pi}{\ln(2)(2+a)b^{a+2}\Gamma(a+1)\rho_t^{\frac{a}{2}+1}} \csc\left(\frac{a\pi}{2}\right) \quad (16)$$

and

$$\mathcal{B}_2 = \frac{\pi}{(a+1)b^{a+1} \ln(2) \Gamma(a+1) \rho_t^{\frac{a+1}{2}}} \sec\left(\frac{a\pi}{2}\right). \quad (17)$$

Therefore, (11) can be approximated as in (15). This concludes the proof. ■

Special case: For  $N = 1$ , the EC can be evaluated according to the following lemma.

**Lemma 2.** *For a single RU RIS, the EC can be obtained as*

$$C_s = \frac{1}{8 \ln(2) \rho_t^2} G_{1,3}^{3,1} \left( \frac{1}{4 \rho_t^2} \middle| \begin{matrix} -1 \\ -1, -1, 0 \end{matrix} \right) \\ - \frac{1}{4 \ln(2) \rho_t} G_{1,3}^{3,1} \left( \frac{1}{4 \rho_t^2} \middle| \begin{matrix} -\frac{1}{2} \\ -\frac{1}{2}, -\frac{1}{2}, -\frac{1}{2} \end{matrix} \right) \\ + \frac{1}{8 \ln(2) \rho_t^2} G_{2,4}^{4,1} \left( \frac{1}{4 \rho_t^2} \middle| \begin{matrix} -1, 0 \\ -1, -1, -1, 1 \end{matrix} \right). \quad (18)$$

*Proof:* Please refer to Appendix C. ■

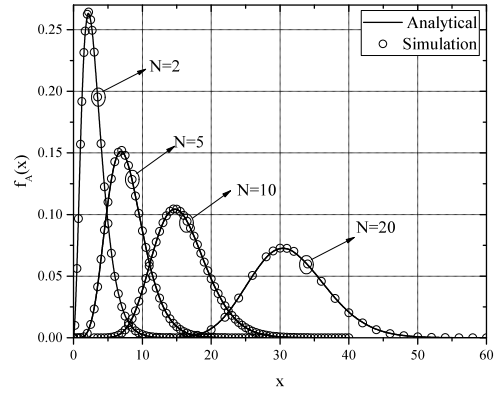


Fig. 2: The PDF of the equivalent e2e channel for different  $N$ .

#### IV. NUMERICAL RESULTS

This section is focused on verifying the theoretical framework through respective Monte Carlo simulations and reporting the EC performance of the RIS-assisted system. Unless otherwise stated, in what follows, we use continuous lines and markers to respectively denote theoretical and simulation results.

Figure 2 illustrates the PDF of the equivalent e2e channel of the RIS-assisted system, for different number of RUs. From this figure, it is observed that the theoretical and simulation results coincide; thus, verifying the presented analytical framework. Additionally, it is observed that, as  $N$  increases, the equivalent e2e channel values also increase. This indicates that by increasing  $N$ , the diversity gain of the RIS-assisted system improves.

Figure 3 depicts the EC as a function of  $\rho_t$ , for different values of  $N$ . In this figure, continuous lines denote the analytical results, the dashed ones stand for the high-SNR approximation, while the dashed-dotted ones represent the high SNR-and- $N$  approximation. We observe that both the high-SNR and the high-SNR- $N$  approximations provides excellent fits even in the

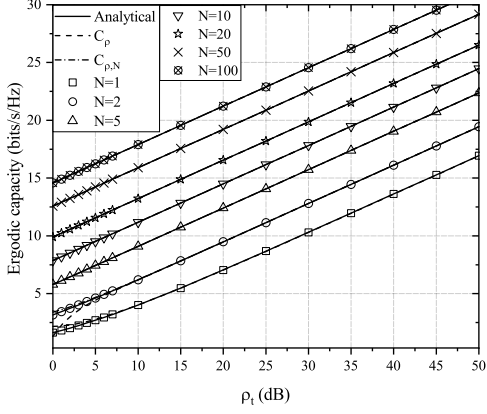


Fig. 3: Capacity vs  $\rho_t$ , for different values of  $N$ .

medium and low transmission SNR regimes. Likewise, it is obvious that, for a fixed  $N$ , as  $\rho_t$  increases, the EC also increases. For instance, for  $N = 2$ , as  $\rho_t$  changes from 5 to 10 dB, the EC improves for about 34.2%. Moreover, for a given  $\rho_t$ , as  $N$  increases, the achievable EC increases. For example, for  $\rho_t = 10$  dB, as  $N$  shifts from 50 to 100, the EC increases for approximately 12.64%. Finally, this figure reveals that, independently of  $\rho_t$ , as  $N$  doubles, the EC increases for about 2 bits/s/Hz.

## V. CONCLUSIONS

This contribution studied the EC of RIS-assisted systems. After obtaining the PDF of the equivalent e2e channel of the RIS-assisted system, we extracted novel closed-form expressions for the EC together with low-complexity tight high-SNR and high- $N$  approximations. The analytical results were compared against respective Monte Carlo simulations, which validated their accuracy and revealed that as the number of RUs increases, the EC also increases. Interestingly, it was observed that as the number of RUs doubles, the EC for about 2 bits/s/Hz.

## APPENDICES

### APPENDIX A

#### PROOF OF LEMMA 1

Since,  $|h_i|$  and  $|g_i|$  are Rayleigh distributed RVs, from (5), it becomes evident that  $A$  is the sum of  $N$  independent and identical double Rayleigh processes, which PDF, according to [26, ch. 2.2.2], can be tightly approximated as the first term of a Laguerre series expansion, i.e., (6). The parameters  $a$  and  $b$  are given in (7), whereas  $k_1$  and  $k_2$  can be evaluated as [26, eq. (2.74)]

$$k_1 = \mathbb{E}[A], \quad (19)$$

and

$$k_2 = 4\mathbb{V}[A]. \quad (20)$$

The expected value of  $A$  can be obtained as

$$\mathbb{E}[A] = \sum_{i=1}^N \mathbb{E}[|h_i||g_i|], \quad (21)$$

or, due the  $|h_i|$  and  $|g_i|$  independency,

$$\mathbb{E}[A] = \sum_{i=1}^N \mathbb{E}[|h_i|] \mathbb{E}[|g_i|]. \quad (22)$$

Likewise,  $|h_i|$  and  $|g_i|$  follow Rayleigh distribution with variances 1; thus,

$$\mathbb{E}[|h_i|] = \mathbb{E}[|g_i|] = \sqrt{\frac{\pi}{2}}. \quad (23)$$

By substituting (23) into (22), we get

$$\mathbb{E}[A] = N \frac{\pi}{2}. \quad (24)$$

Similarly, the variance of  $A$  can be computed as

$$\mathbb{V}[A] = N \left(1 - \frac{\pi^2}{16}\right). \quad (25)$$

By substituting (24) and (25) into (19) and (20), we obtain (8). This concludes the proof.

## APPENDIX B

### PROOF OF THEOREM 1

The EC is defined as

$$C = \mathbb{E}[\log_2(1 + \rho)], \quad (26)$$

which can be equivalently written as

$$C = \int_0^\infty \log_2(1 + \rho_t y^2) f_A(y) dy. \quad (27)$$

By substituting (6) into (27), the EC can be rewritten as

$$C = \frac{x^a}{b^{a+1}\Gamma(a+1)} \int_0^\infty \exp\left(-\frac{y}{b}\right) \log_2(1 + \rho_t y^2) dy, \quad (28)$$

or

$$C = \frac{1}{b^{a+1} \ln(2) \Gamma(a+1)} \mathcal{K}, \quad (29)$$

where

$$\mathcal{K} = \int_0^\infty y^a \exp\left(-\frac{y}{b}\right) \ln(1 + \rho_t y^2) dy. \quad (30)$$

Based on [24, eq. (15.1.1)], (30) can be written as

$$\mathcal{K} = \rho_t \int_0^\infty y^{a+2} \exp\left(-\frac{y}{b}\right) {}_2F_1(1, 1; 2; -\rho_t y^2) dy, \quad (31)$$

which, after applying integration by parts as well as [27, eq. (07.23.21.0015.01)], can be expressed as in (32), given at the top of the following page. In addition, by substituting (32) into (29), and after some algebraic manipulations, we extract (33), given at the top of the following page. Finally, by taking into account that  $\frac{\Gamma(x+n)}{\Gamma(x)} = (x)_n$ , (33) can be rewritten as in (10). This concludes the proof.

$$\begin{aligned}
\mathcal{K} = & 4ab^{a+3}\Gamma(a)\rho_t \ln(b\sqrt{\rho_t}) + 6a^2b^{a+3}\Gamma(a)\rho_t \ln(b\sqrt{\rho_t}) + 2a^3b^{a+3}\Gamma(a)\rho_t \ln(b\sqrt{\rho_t}) \\
& + 2a(a+1)(a+2)b^{a+3}\Gamma(a)F_0(3+a) - \frac{\pi}{(4+a)b\rho_t^{\frac{a}{2}+1}} \csc\left(\frac{a\pi}{2}\right) {}_1F_2\left(2+\frac{a}{2}; \frac{3}{2}, 3+\frac{a}{2}, -\frac{1}{4b^2\rho_t}\right) \\
& - \frac{\pi}{(a+3)\rho_t^{\frac{a+1}{2}}} \sec\left(\frac{a\pi}{2}\right) {}_1F_2\left(\frac{a+3}{2}; \frac{1}{2}, \frac{a+5}{2}, -\frac{1}{4b^2\rho_t}\right) + ab^{a+1}\Gamma(a) {}_2F_3\left(1, 1; 2, \frac{1-a}{2}, -\frac{a}{2}, -\frac{1}{4b^2\rho_t}\right)
\end{aligned} \tag{32}$$


---

$$\begin{aligned}
C = & 4ab^2 \frac{\Gamma(a)}{\Gamma(a+1)} \rho_t \log_2(b\sqrt{\rho_t}) + 6a^2b^2 \frac{\Gamma(a)}{\Gamma(a+1)} \rho_t \log_2(b\sqrt{\rho_t}) + 2a^3b^2 \frac{\Gamma(a)}{\Gamma(a+1)} \rho_t \log_2(b\sqrt{\rho_t}) \\
& + \frac{2}{\ln(2)} a(a+1)(a+2)b^2 \frac{\Gamma(a)}{\Gamma(a+1)} F_0(3+a) \\
& - \frac{\pi}{\ln(2)(4+a)b^{a+2}\Gamma(a+1)\rho_t^{\frac{a}{2}+1}} \csc\left(\frac{a\pi}{2}\right) {}_1F_2\left(2+\frac{a}{2}; \frac{3}{2}, 3+\frac{a}{2}, -\frac{1}{4b^2\rho_t}\right) \\
& - \frac{\pi}{(a+3)b^{a+1}\ln(2)\Gamma(a+1)\rho_t^{\frac{a+1}{2}}} \sec\left(\frac{a\pi}{2}\right) {}_1F_2\left(\frac{a+3}{2}; \frac{1}{2}, \frac{a+5}{2}, -\frac{1}{4b^2\rho_t}\right) \\
& + \frac{a}{\ln(2)} \frac{\Gamma(a)}{\Gamma(a+1)} {}_2F_3\left(1, 1; 2, \frac{1-a}{2}, -\frac{a}{2}, -\frac{1}{4b^2\rho_t}\right)
\end{aligned} \tag{33}$$


---

## APPENDIX C

### PROOF OF LEMMA 2

Based on (26), the EC can be obtained as

$$C_s = \int_0^\infty \log_2(1 + \rho_t x) f_\rho^s(x) dx, \tag{34}$$

or equivalently

$$C_s = \frac{1}{\ln(2)} \int_0^\infty \ln(1 + \rho_t x^2) f_A^s(x) dx, \tag{35}$$

which, with the aid of (6), can be expressed as

$$C_s = \frac{1}{4\ln(2)\rho_t} C_1 - \frac{1}{2\ln(2)\sqrt{\rho_t}} C_2 + \frac{1}{4\ln(2)\rho_t} C_3, \tag{36}$$

where

$$C_1 = \int_0^\infty K_0\left(\sqrt{\frac{x}{\rho_t}}\right) \ln(1 + \rho_t x) dx, \tag{37}$$

$$C_2 = \int_0^\infty x^{-1/2} K_1\left(\sqrt{\frac{x}{\rho_t}}\right) \ln(1 + \rho_t x) dx \tag{38}$$

and

$$C_3 = \int_0^\infty K_2\left(\sqrt{\frac{x}{\rho_t}}\right) \ln(1 + \rho_t x) dx. \tag{39}$$

Moreover, by using [23, eq. (8.352/2)], (37)-(39) can be equivalently written as

$$C_1 = \rho_t \int_0^\infty x K_0\left(\sqrt{\frac{x}{\rho_t}}\right) {}_2F_1(1, 1; 2; \rho_t x) dx, \tag{40}$$

$$C_2 = \rho_t \int_0^\infty x^{1/2} K_1\left(\sqrt{\frac{x}{\rho_t}}\right) {}_2F_1(1, 1; 2; \rho_t x) dx \tag{41}$$

and

$$C_3 = \rho_t \int_0^\infty x K_2\left(\sqrt{\frac{x}{\rho_t}}\right) {}_2F_1(1, 1; 2; \rho_t x) dx. \tag{42}$$

Moreover, with the aid of [28, eq. (03.04.26.0009.01)] and [29, eq. (17)], (40)-(42) can be respectively written as

$$\begin{aligned}
C_1 = & \frac{\rho_t}{2} \int_0^\infty x G_{0,2}^{2,0}\left(\frac{x}{4\rho_t} \middle| 0, 0\right) \\
& \times G_{2,2}^{1,2}\left(\rho_t x \middle| \begin{matrix} 0, 0 \\ 0, -1 \end{matrix}\right) dx,
\end{aligned} \tag{43}$$

$$\begin{aligned}
C_2 = & \frac{\rho_t}{2} \int_0^\infty x^{1/2} G_{0,2}^{2,0}\left(\frac{x}{4\rho_t} \middle| \frac{1}{2}, -\frac{1}{2}\right) \\
& \times G_{2,2}^{1,2}\left(\rho_t x \middle| \begin{matrix} 0, 0 \\ 0, -1 \end{matrix}\right) dx
\end{aligned} \tag{44}$$

and

$$\begin{aligned}
C_3 = & \frac{\rho_t}{2} \int_0^\infty x G_{0,2}^{2,0}\left(\frac{x}{4\rho_t} \middle| 1, -1\right) \\
& \times G_{2,2}^{1,2}\left(\rho_t x \middle| \begin{matrix} 0, 0 \\ 0, -1 \end{matrix}\right) dx,
\end{aligned} \tag{45}$$

which, by applying [30, ch. 2.3], can be analytically evaluated as

$$C_1 = \frac{1}{2\rho_t} G_{1,3}^{3,1}\left(\frac{1}{4\rho_t^2} \middle| \begin{matrix} -1 \\ -1, -1, 0 \end{matrix}\right), \tag{46}$$

$$C_2 = \frac{1}{2\sqrt{\rho_t}} G_{1,3}^{3,1}\left(\frac{1}{4\rho_t^2} \middle| \begin{matrix} -\frac{1}{2} \\ -\frac{1}{2}, -\frac{1}{2}, -\frac{1}{2} \end{matrix}\right) \tag{47}$$

and

$$C_3 = \frac{1}{2\rho_t} G_{2,4}^{4,1} \left( \frac{1}{4\rho_t^2} \middle| \begin{matrix} -1, 0 \\ -1, -1, -1, 1 \end{matrix} \right). \quad (48)$$

Finally, by substituting (46)-(48) into (36), we extract (18). This concludes the proof.

## REFERENCES

- [1] W. Saad, M. Bennis, and M. Chen, "A vision of 6G wireless systems: Applications, trends, technologies, and open research problems," *IEEE Netw.*, pp. 1–9, Oct. 2019.
- [2] A.-A. A. Boulgeorgos and G. K. Karagiannidis, "Low-cost cognitive radios against spectrum scarcity," *IEEE Technical Committee on Cognitive Networks Newsletter*, vol. 3, no. 2, pp. 30–34, Nov. 2017.
- [3] A.-A. A. Boulgeorgos, A. Alexiou, T. Merkle, C. Schubert, R. Elschner, A. Katsiotis, P. Stavrianos, D. Kritharidis, P. K. Chartsias, J. Kokkonen, M. Juntti, J. Lehtomäki, A. Teixeira, and F. Rodrigues, "Terahertz technologies to deliver optical network quality of experience in wireless systems beyond 5G," *IEEE Commun. Mag.*, vol. 56, no. 6, pp. 144–151, Jun. 2018.
- [4] A.-A. A. Boulgeorgos, A. Alexiou, D. Kritharidis, A. Katsiotis, G. Ntouni, J. Kokkonen, J. Lehtomäki, M. Juntti, D. Yankova, A. Mokhtar, J.-C. Point, J. Machodo, R. Elschner, C. Schubert, T. Merkle, R. Ferreira, F. Rodrigues, and J. Lima, "Wireless terahertz system architectures for networks beyond 5G," *TER-RANOVA CONSORTIUM*, White paper 1.0, Jul. 2018.
- [5] C. Pan, H. Ren, K. Wang, W. Xu, M. El-kashlan, A. Nallanathan, and L. Hanzo, "Intelligent reflecting surface for multicell mimo communications," *arXiv preprint arXiv:1907.10864*, 2019.
- [6] A.-A. A. Boulgeorgos and G. K. Karagiannidis, "Energy detection in full-duplex systems with residual RF impairments over fading channels," *IEEE Wireless Commun. Lett.*, vol. 7, no. 2, pp. 246–249, Apr. 2018.
- [7] A.-A. A. Boulgeorgos, E. Papatotiriou, and A. Alexiou, "A distance and bandwidth dependent adaptive modulation scheme for THz communications," in *19th IEEE International Workshop on Signal Processing Advances in Wireless Communications (SPAWC)*, Kalamata, Greece, Jul. 2018.
- [8] A.-A. A. Boulgeorgos, S. Goudos, and A. Alexiou, "Users association in ultra dense THz networks," in *IEEE International Workshop on Signal Processing Advances in Wireless Communications (SPAWC)*, Kalamata, Greece, Jun. 2018.
- [9] A.-A. A. Boulgeorgos, "Interference mitigation techniques in modern wireless communication systems," Ph.D. dissertation, Aristotle University of Thessaloniki, Thessaloniki, Greece, Sep. 2016.
- [10] Y. Han, W. Tang, S. Jin, C. Wen, and X. Ma, "Large intelligent surface-assisted wireless communication exploiting statistical CSI," *IEEE Trans. Veh. Technol.*, vol. 68, no. 8, pp. 8238–8242, Aug. 2019.
- [11] A.-A. A. Boulgeorgos, E. N. Papatotiriou, and A. Alexiou, "Analytical performance evaluation of thz wireless fiber extenders," in *IEEE 30th Annual International Symposium on Personal, Indoor and Mobile Radio Communications (PIMRC)*, Sep. 2019, pp. 1–6.
- [12] E. N. Papatotiriou, J. Kokkonen, A.-A. A. Boulgeorgos, J. Lehtomäki, A. Alexiou, and M. Juntti, "A new look to 275 to 400 ghz band: Channel model and performance evaluation," in *IEEE International Symposium on Personal, Indoor and Mobile Radio Communications (PIMRC)*, Bologna, Italy, Sep. 2018.
- [13] A.-A. A. Boulgeorgos and A. Alexiou, "Performance analysis of reconfigurable intelligent surface-assisted wireless systems and comparison with relaying," *IEEE Access*, vol. 8, pp. 94463–94483, May 2020.
- [14] M. D. Renzo, M. Debbah, D.-T. Phan-Huy, A. Zappone, M.-S. Alouini, C. Yuen, V. Sciancalepore, G. C. Alexandropoulos, J. Hoydis, H. Gacanin, J. d. Rosny, A. Bounceur, G. Lerosee, and M. Fink, "Smart radio environments empowered by reconfigurable ai meta-surfaces: An idea whose time has come," *EURASIP Journal on Wireless Communications and Networking*, vol. 2019, no. 1, pp. 1–20, May 2019.
- [15] A. C. Tasolamprou, A. Ptilakis, S. Abadal, O. Tsilipakos, X. Timoneda, H. Taghvaei, M. Sajjad Mirmoosa, F. Liu, C. Liaskos, A. Tsoliariadou, S. Ioannidis, N. V. Kantartzis, D. Manassis, J. Georgiou, A. Cabellos-Aparicio, E. Alarcn, A. Pitsillides, I. F. Akyildiz, S. A. Tretyakov, E. N. Economou, M. Kafesaki, and C. M. Soukoulis, "Exploration of intercell wireless millimeter-wave communication in the landscape of intelligent metasurfaces," *IEEE Access*, vol. 7, pp. 122931–122948, Aug. 2019.
- [16] Q. Wu and R. Zhang, "Intelligent reflecting surface enhanced wireless network: Joint active and passive beamforming design," in *IEEE Global Communications Conference (GLOBECOM)*, Dec 2018, pp. 1–6.
- [17] E. Basar, M. Di Renzo, J. De Rosny, M. Debbah, M. Alouini, and R. Zhang, "Wireless communications through reconfigurable intelligent surfaces," *IEEE Access*, vol. 7, pp. 116753–116773, 2019.
- [18] E. Basar, "Transmission through large intelligent surfaces: A new frontier in wireless communications," in *Eur. Conf. Netw. Commun. (EuCNC)*, Valencia, Spain, Jun. 2019, pp. 1–6.
- [19] V. C. Thirumavalavan and T. S. Jayaraman, "BER analysis of reconfigurable intelligent surface assisted downlink power domain NOMA system," in *International Conference on Communication Systems & NETWORKS (COMSNETS)*, Jan. 2020.
- [20] M. Jung, W. Saad, Y. Jang, G. Kong, and S. Choi, "Reliability analysis of large intelligent surfaces (LISs): Rate distribution and outage probability," *IEEE Wireless Commun. Lett.*, vol. 8, no. 6, pp. 1662–1666, Dec. 2019.
- [21] M. D. Renzo, K. Ntontin, J. Song, F. H. Danufane, X. Qian, F. Lazarakis, J. de Rosny, D. T. Phan-Huy, O. Simeone, R. Zhang, M. Debbah, G. Lerosee, M. Fink, S. Tretyakov, and S. Shamai, "Reconfigurable intelligent surfaces vs. relaying: Differences, similarities, and performance comparison," 2019.
- [22] E. Bjornson, O. Ozdogan, and E. G. Larsson, "Intelligent reflecting surface versus decode-and-forward: How large surfaces are needed to beat relaying?" *IEEE Wireless Commun. Lett.*, vol. 9, no. 2, pp. 244–248, Feb. 2020.
- [23] I. S. Gradshteyn and I. M. Ryzhik, *Table of Integrals, Series, and Products*, 6th ed. New York: Academic, 2000.
- [24] M. Abramowitz and I. A. Stegun, *Handbook of Mathematical Functions with Formulas, Graphs, and Mathematical Tables*, 9th ed. New York: Dover Publications, 1972.
- [25] I. Z. Kovacs, P. C. F. Eggers, K. Olesen, and L. G. Petersen, "Investigations of outdoor-to-indoor mobile-to-mobile radio communication channels," in *IEEE 56th Vehicular Technology Conference*, vol. 1, Sep. 2002, pp. 430–434.
- [26] S. Primak, V. Kontorovich, and V. Lyandres, *Stochastic Methods and Their Applications to Communications Stochastic Differential Equations Approach*. West Sussex, England: John Wiley & Sons, Ltd, 2004.
- [27] Wolfram site, "Tree. From MathWorld—A Wolfram Web Resource," Oct. 2001, last visited on 14/11/2019. [Online]. Available: <http://functions.wolfram.com/HypergeometricFunctions/Hypergeometric2F1/21/02/02/0001/>
- [28] "The wolfram functions site," <http://functions.wolfram.com/03.04.26.0009.01>. [Online]. Available: <http://functions.wolfram.com/03.04.26.0009.01>
- [29] V. S. Adamchik and O. I. Marichev, "The algorithm for calculating integrals of hypergeometric type functions and its realization in REDUCE system," in *Proceedings of the International Symposium on Symbolic and Algebraic Computation*, ser. ISSAC '90. New York, NY, USA: ACM, Aug. 1990, pp. 212–224.
- [30] A. M. Mathai, R. K. Saxena, and H. J. Haubold, *The H-Function: Theory and Applications*. New York Dordrecht Heidelberg London: Springer, 2010.